Strain-tunable optical valves at T-junction waveguides in photonic crystals

Natalia Malkova and Venkatraman Gopalan
Materials Research Institute, Pennsylvania State University, University Park, Pennsylvania 16802, USA
(Received 9 July 2003; revised 11 September 2003; published 22 December 2003)

We propose to use tunable splitting of a degenerate photon state inside the band gap of a photonic crystal for the design of active tunable photonic crystal circuits. The effect we exploit is analogous to the static Jahn-Teller effect in solids. We demonstrate that effect is tunable by the symmetry and magnitude of the lattice distortion. Using this effect, we design an optical valve that controls the resonant coupling of the photon modes at the corner of a T-junction waveguide structure.

DOI: 10.1103/PhysRevB.68.245115 PACS number(s): 71.70.Ej, 42.70.Qs, 41.20.Jb, 42.79.Gn

I. INTRODUCTION

Photonic crystals formed by periodic modulation of dielectric constant are a promising platform for the control and manipulation of the propagation of photons.[1] Particularly, waveguide bends with negligible reflection are of great interest because they are crucial for realizing photonic crystal circuits. Therefore there is a growing interest in developing photonic crystal-based waveguide components which can guide and bend light either along a line defect (a row of missing rods)[2] or through coupled cavities.[3] In the former case, the light is confined in the direction perpendicular to the waveguide axis, and photons can propagate in the direction parallel to the axis of the missing rods. In the latter case, called coupled cavity waveguides, the guided electromagnetic waves are tightly confined at each defect site, and photons can propagate by hopping, due to interaction between the neighboring evanescent cavity modes.[4] The most important feature of the these coupled cavity waveguides is the possibility of constructing lossless and reflectionless bends.[5] This ability has a crucial role in overcoming the problem of guiding light around sharp corners in optical circuits.[2]

On the other hand, for application in optical devices, it is important to realize the tunability of the photonic crystals. A tunable light propagation has been recently reported[6] in Y-shaped waveguides based on two-dimensional photonic crystals with triangular lattice using liquid crystals as linear defects. In this paper, we propose to use a tunable splitting of the degeneracy of a defect state, in order to control the defect mode coupling at the corner of a coupled cavity waveguide structure. The effect that we exploit is analogous to the Jahn-Teller effect in solids.[7] It is based on the symmetrical analysis of the splitting of the degenerate states by a convenient distortion of the lattice.[8] It is natural to expect that the control of the frequency of the corner defect should provide an opportunity for tunable light propagation through the bent waveguide. The application of the effect for designing a 90°-bend waveguide has been recently shown.[9] The aim of this paper is to show an application of the effect for designing a coupled cavity, T-shaped waveguide structure.

The paper is organized as follows. In Sec. II, we provide a short sketch of the static Jahn-Teller effect in the photonic crystals. We present a group theory analysis of the degenerate level splitting inside the band gap of the photonic crystal. Then, in Sec. III, we apply the developed approach for the design of a T-shaped coupled cavity waveguide. Finally, we summarize the results in the conclusion section.

II. STATIC JAHN-TELLER EFFECT IN PHOTONIC CRYSTAL

We refer to our paper, Ref. 10, for a detailed analysis of the static Jahn-Teller effect in photonic crystals, giving here only a brief sketch of the central idea.

As a model material, we consider a two-dimensional square photonic lattice doped by a defect rod. The point-group symmetry of the square lattice is C_{4v}. If the defect rod is localized at the site of the lattice, then by symmetry it may be described both by the one-dimensional $A_{1,2}$, $B_{1,2}$ and two-dimensional E irreducible representations of the group C_{4v}.[11] One-dimensional irreducible representations result in nondegenerate photon states. The two-dimensional representation gives a doubly degenerate state represented by the two 1×2 column basis vectors having the shape of the $|p_x\rangle$ and $|p_y\rangle$ orbitals.[11] This is the state under our consideration for two reasons. First, we want to use the splitting of the doubly degenerate state for tuning light propagation. Second, in the case of the coupled cavity waveguide, this state, being described by the $|p_x\rangle$ and $|p_y\rangle$ orbitals, gives a good coupling for light propagation along the x and y axes, respectively.

In solid-state physics, when studying the Jahn-Teller effect, a crystal subject to lattice vibrations is considered.[12] The dynamic Jahn-Teller effect in the photonic crystals has been studied in Ref. 8. For the goals of this paper, we limit ourselves to studying a photonic crystal subject to static distortion of the lattice, which in the mathematical formulation of the problem will be described by the perturbation potential V. In the framework of the group theory, all distortions of the lattice can be presented as a sum of the normal irreducible distortions. For the square lattice with the in-site defect atom, there are A_1, $B_{1,2}$, and E normal irreducible distortions that are allowed.[12] All the distortions are presented in Fig. 1. It has been shown[8] that in application to the splitting of the E-photon state, only irreducible distortions B_1 and B_2 are involved [Figs. 1(b) and (c)]. The total symmetrical distortion A_1 [Fig. 1(a)] results in equal shift of the double degenerate state without lifting the degeneracy, while the E distortion [Fig. 1(d)], characterized by the two-dimensional irreducible representation, can lift the degeneracy only in the second order of the perturbation theory. In the case of the B_1

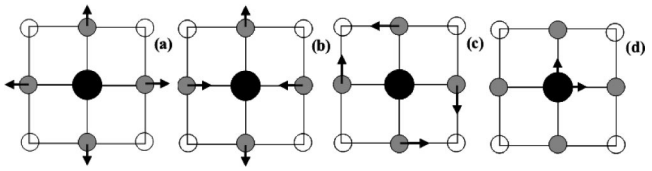

FIG. 1. The Jahn-Teller cell of the square lattice distorted by the A_1 (a), B_1 (b), B_2 (c), and E (d) perturbations.

lattice distortion, the *E*-photonic mode, which in the unperturbed lattice has the frequency $\omega=\omega_0$, splits into two levels,

$$\omega_{1,2}^{B1}=\omega_0\pm V_{xx}^{B_1}, \tag{1}$$

where $V_{xx}^{B1}=\langle p_x|V^{B1}|p_x\rangle$ is the matrix element of the perturbative potential, described by symmetry of the B_1 distortion. It is of importance that the eigenvectors of the split states, in this case, should satisfy the symmetry of the $|p_x\rangle$ and $|p_y\rangle$ orbitals. For the B_2 distortion, the splitting gives $|p_x\pm p_y\rangle$ orbitals with the energy

$$\omega_{1,2}^{B2}=\omega_0\pm V_{xy}^{B_2}, \tag{2}$$

where $V_{xy}^{B2}=\langle p_x|V^{B2}|p_y\rangle$ is the matrix element for the B_2 distortion.

The following aspects are of importance for further analysis. First, in the first approximation of the perturbation theory, the perturbative potential has a linear dependence on the magnitude of lattice distortion. Because of this the splitting of the doubly degenerate level should be a linear function of the magnitude of the lattice distortion, $\Delta\omega=2V^{\alpha}=v^{\alpha}\Delta r$, with the deformation potential v^{α} as a scaling coefficient. The deformation potential v^{α} can be easily found from the supercell plane-wave calculations.[8] Second, the symmetry of the split photon states can be controlled by the symmetry of the lattice distortion. This means that by choosing the B_1 or B_2 perturbation as a lattice distortion, we can either get the $|p_x\rangle$ and $|p_y\rangle$ states or $|p_x\pm p_y\rangle$ symmetry of the split states, respectively. Both of these features will be shown to be of importance in our design of the complex shaped coupled cavity waveguide.

III. PROPAGATION OF THE LIGHT THROUGH T-SHAPED COUPLED CAVITY WAVEGUIDE

The analysis presented above allows the selection of the perturbation of the lattice, resulting in a desirable magnitude and symmetry of the defect state splitting. Therefore we can tune the splitting of the defect mode, both by the frequency and by symmetry. We now propose the T-shaped coupled cavity waveguide, in which at the corner we place the so-called Jahn-Teller cell. We consider two systems in which the B_1 and B_2 perturbations are working.

As a model crystal, we will study a square photonic crystal of dielectric rods, embedded in air with a lattice constant *a*, the radius of the rods $r=0.2a$, and the dielectric constant $\epsilon_r=11.9$. Here, only modes with odd (TM-like) symmetry are considered, since that is the symmetry of the bands exhibiting a gap for the square lattice. We study the defect state created by the defect rod with radius $r_d=0.3a$ and the same dielectric constant $\epsilon_d=11.9$ as the other rods. We are interested in the doubly degenerate defect state lying inside the first band gap. We consider distortions of the lattice within the limits $\Delta r=0-0.3a$, keeping in mind that only small distortions ($\Delta r\ll a$) allow for the validity of the linear approximation of the perturbative potential.

To analyze these structures, we use the finite difference time domain (FDTD) simulation, following the technique described in Ref. 13. Our computational domain contained 15 $\times$17 unit cells. Each unit cell was divided into 20$\times$20 discretization grid cells. The computational domain was surrounded by perfect matched layers, with the thickness corresponding to ten layers of the discretization grid. The total number of the time steps was 100 000 with each time step $\Delta t=1/(2\Delta xc)$. The source was simulated as a Gaussian beam in time domain and in the coordinate space with the width of the beam equal to 40 grid cells. In order to calculate the transmission of the structure, we collect the signal at the output of the waveguide structure and compare these data with the reference signal collected at the input of the structure,[14] determining the transmittance of the structure as a ratio between the transmitted and incident (reference) light intensities.

A. B_1 mode

At first, we consider the structure, shown in the inset of Fig. 2(a). This waveguide consists of three arms. We will call the first arm before the corner going along the *x* axis as arm 1. The arms after the corner will be named arm 2 for the branch going along the *x* axis, and arm 3 for the branch going along the *y* axis. From the geometry of this structure, we can immediately guess that we can tune the propagation of the light through the different arms if we place at the corner a Jahn-Teller cell deformed by the B_1 perturbation, which is shown in Fig. 1(b). We will study the waveguide with the distortion of the corner cell in the region $\Delta r/a=0:\pm 0.3$. Here, we define the positive distortion of the lattice as shown in Fig. 1(b) and a negative distortion that reverses the displacements. We compare the transmission of the structure at the two output ports, shown in the inset of Fig. 2(a).

We present in Fig. 2 the computed transmission coefficient inside the band gap for the structure with $\Delta r/a=0$, 0.08, and 0.10 at port 2 (a) and for the structure with $\Delta r/a=0$, 0.10 and -0.03 at port 1 (b), respectively.[15] We observe an increased transmission of the light at port 2 when $\Delta r>0$, while the transmission decreases for $\Delta r<0$. Conversely, the transmission at port 1 increases when $\Delta r<0$ and decreases when $\Delta r>0$. We note that the transmission spectrum at port 2 at $\Delta r/a=0.10$ is characterized by a very sharp peak with the width $\delta\omega\sim 10^{-3}$ (in relative unites). Here and hereafter, we will use the relative dimensionless units for frequency, determined by $\tilde{\omega}=\omega a/(2\pi c)$. Figure 3 shows the maximum of the relative transmission of the structure at port 1 (solid line) and at port 2 (dashed line) as a function of the lattice distortion. We note from Fig. 3 that at port 2 the effect shows a resonant behavior with the maximum at

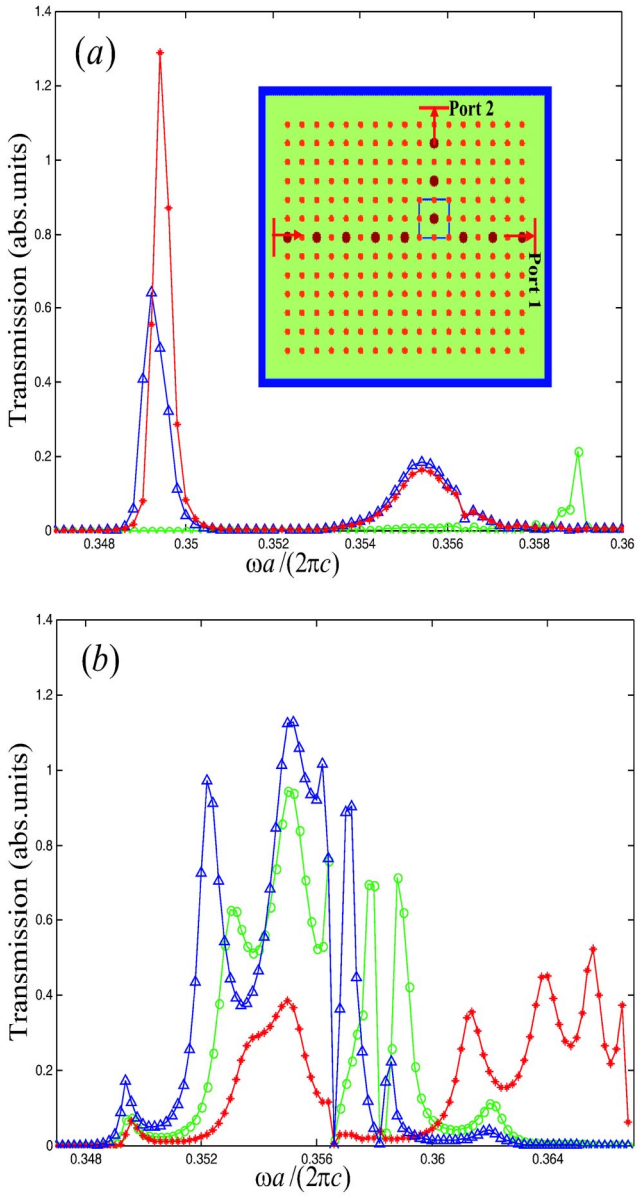

FIG. 2. (Color online) The relative transmission intensity inside the band gap for the structures shown in the inset with $\Delta r/a=0$ (circle marker), 0.08 (triangular marker), 0.10 (star marker) at port 2 (a) and with $\Delta r/a=0$ (circle marker), 0.10 (star marker), -0.03 (triangular marker), at port 1 (b). The inset shows the structure studied with the B_1 distortion of the corner cell. The Jahn-Teller corner cell, the perfect matched boundaries as well as, the source and two ports are overlaid.

$\Delta r/a=0.10$ (solid line), while at port 1, the enhancement of the transmission is not so sharp, with the maximum at $\Delta r/a=-0.03$. Figure 4 presents the pattern of the z component of the electric field in the frequency domain for the resonant frequency $\omega=0.349$ at $\Delta r/a=0$ (a), 0.05 (c), 0.10 (d), and for $\omega=0.355$ at $\Delta r/a=-0.03$ (b).

Analyzing this system in terms of the tight-binding model,[5] we note the following. The doubly degenerate state of the linear chain generates two bands $\omega_{\parallel}=\omega_0\pm\beta_{\parallel}$ and $\omega_{\perp}=\omega_0\pm\beta_{\perp}$. Here $\beta_{\parallel}$ is the coupling coefficient between the nearest $|p_x\rangle$ (or $|p_y\rangle$) states located along the x (or y) axis, and $\beta_{\perp}$ is the coupling coefficient between the nearest $|p_y\rangle$ (or $|p_x\rangle$) states located along the x (or y) axis. The band $\omega_{\parallel}$ is characterized by the symmetry of the p orbital parallel to the defect chain, that is $|p_x\rangle$ for the first and second waveguide arms and $|p_y\rangle$ for the third bent arm. The band $\omega_{\perp}$ is characterized by the orthogonal p-orbital (with respect to the first band), that is, the $|p_y\rangle$ for arms 1 and 2 and $|p_x\rangle$ orbitals for arm 3. Because of far-reduced coupling between the $|p_y\rangle$ states as compared to that between the $|p_x\rangle$ states $\beta_{\perp}<\beta_{\parallel}$ at any point located on the x axis. The FDTD simulations show that for the defect crystal studied $2\beta_{\parallel}=0.01$ and $2\beta_{\perp}=0.001$ (in relative units). It is of importance for the linear chain with a finite number of sites n that the spectrum of each band consists of the n levels separated by $\sim 2\beta_{\parallel(\perp)}/(n-1)$.

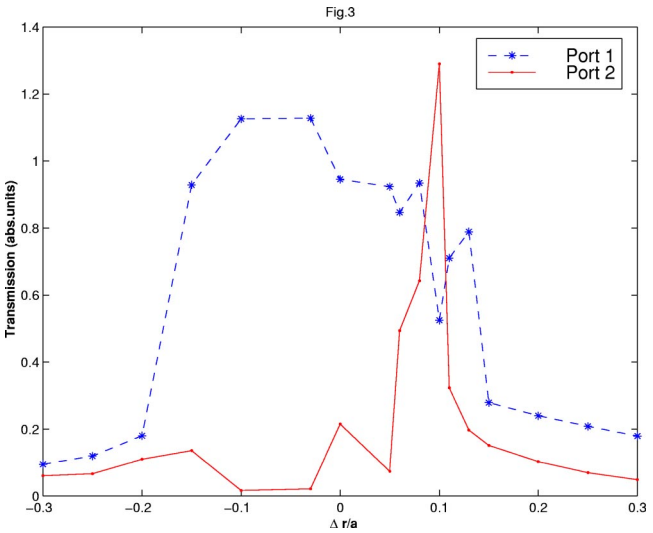

FIG. 3. Computed maximum of the relative transmission coefficient of the structure shown in the inset of Fig. 2(a), as a function of the lattice distortion at port 1 (dashed line) and at port 2 (solid line).

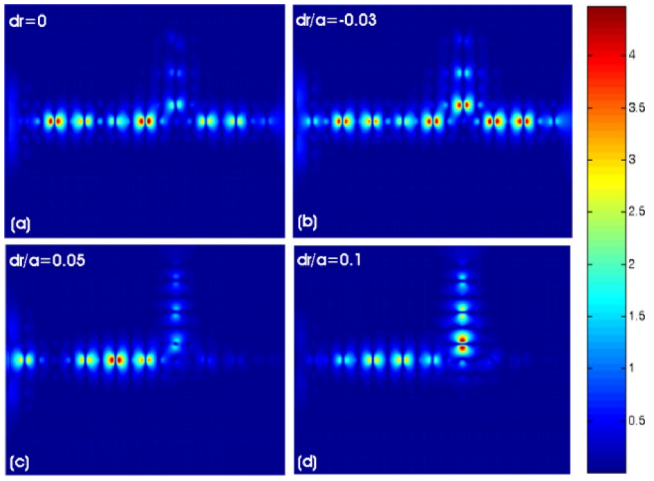

FIG. 4. (Color online) The pattern of the z component of the electric field in the frequency domain for the resonant frequency $\omega=0.349$ at $\Delta r/a=0$ (a), 0.05 (c), 0.10 (d), and for $\omega=-0.355$ at $\Delta r/a=-0.03$ (b).

It is obvious that the strongest coupling of the cavity modes, and because of this the highest transmission at port 1, will be for the case when the light propagates through the p_x bands before and after the split corner. On the other hand, at port 2, the strongest transmission should be expected in the case if light propagates through the p_x band before the bend and through the p_y band after the bend. However, since the distance between the two bands is small, having overlap at some wave vectors, the light can tunnel at the corner from the p_x band of arm 1 to p_x band of arm 2, without flipping the symmetry. But in such a case, a lot of energy is lost, first, because of nonzero reflectivity from the corner and, second, because of poor coupling between the p_x modes after bending. The pattern of the E_z field, shown in Fig. 4(a), provides evidence that such a propagation of the light is preferable when $\Delta x=0$. As a result, the transmission of such a structure at port 2 will be small [the line connecting circular symbols in Fig. 2(a)]. However, the transmission at port 1 cannot be 100% [the line connecting circular markers in Fig. 2(b)] because some part of the energy flow will be transferred along arm 3.

Now, if the corner cell is distorted by the B_1 perturbation, the $|p_x\rangle$ and $|p_y\rangle$ states of the corner defect are separated by $\Delta\omega=2V^{B1}=v^{B1}\Delta r$. We will use the value $v^{B1}=0.1$, obtained in Ref. 8 by means of supercell plane-wave calculations.

First, we note that the corner defect of this structure should be considered as a part of arm 3. Because of this, for small distortion of the lattice such that $v^{B1}\Delta r \ll 2\beta_{\|}$, the effect of the lattice distortion on the spectrum of arm 3 is small. The band spectrum will still be governed by the coupling parameter β. When $\Delta r \geqslant 2\beta_{\|}/v^{B1}$, the corner defect becomes independent of the other defects in arm 3. Its spectrum will be mostly governed by the lattice distortion, giving two split levels with strongly localized $|p_x\rangle$ and $|p_y\rangle$ wave functions. For a positive lattice distortion, the $|p_x\rangle$ state of the corner defect shifts up in frequency, while the $|p_y\rangle$ state goes down, and vice versa for the oppositely directed distortion. If the $|p_x\rangle$ state of the corner defect goes up in frequency, then as soon as $\Delta r v^{B1} > 2\beta_{\perp}$, this results in lowering the probability for tunneling through this state without flipping the symmetry. If simultaneously, the $|p_y\rangle$ state goes down, coming closer to the highly transmitted levels of each of the waveguide arms, then the transmission through the corner to port 2 should increase. Resonant transmission at port 2 will be reached when the reflectivity from the corner is equal to zero and when the coupling between the propagating modes is at a maximum. In the framework of the tight-binding model it has been shown[16] that the reflectivity from the corner is proportional to the second order of the coupling matrix elements between the next-nearest neighbors in the defect chain and to the detuning from the resonance frequency. This means that the resonance should be observed when the $|p_y\rangle$ state of the corner defect is matched in frequency with the lowest level of the $\omega_{\|}$ band of the first arm, $\omega_{\|}^{m}=\omega_0-\beta_{\|}$. Since the frequency of the distorted E state of the corner defect is equal to $\omega_{1,2}^{c}=\omega_0\pm v^{B1}\Delta r/2$, then the resonant condition $\omega_{1,2}^{c}=\omega_{\|}^{m}$ gives $v^{B1}\Delta r=2\beta_{\|}$. The width of the resonant peak is determined by the width of the split $|p_y\rangle$ corner defect state. Taking the known values $2\beta_{\|}=0.01$ and $v^{B1}=0.1$, we find that the resonance should be observed at $\Delta r/a\sim 0.1$. This value is in good agreement with the FDTD experiment. For $\Delta r<0$, the $|p_y\rangle$ state of the corner defect goes up in frequency. As a result, the resonant condition for transmission at port 2 fails, but this leads to an increased transmission at port 1 [line with triangular markers in Fig. 2(b)]. Pattern of the E_z field for $\Delta r/a=0.05$, 0.10, and -0.03 presented in Figs. 4(b)–(d) provides support for this analysis.

B. B_2 mode

Next, we present another structure of the coupled cavity waveguide shown in the inset of Fig. 5(a). We will again select 3 arms and one corner defect in this structure. Now the geometry of the structure suggests that the best coupling between arms 1 and 3 can be achieved if the corner Jahn-Teller cell is distorted by a B_2 perturbation, as shown in Fig. 1(c). Because of the symmetry of the structure, we analyze this waveguide structure only for $\Delta r>0$.

We show in Fig. 5 the relative transmission intensity inside the band gap for the structures with (a) $\Delta r/a=0$, 0.05, 0.13, and 0.25 at port 2 and for the structure with (b) $\Delta r/a=0$, 0.1, 0.13 and 0.25 at port 1. We observe increasing the transmission of the light at port 2 when $\Delta r>0$. However, in comparison with the first structure, the transmission at port 1 does not decrease. The maximum shifts only in frequency. It is of importance that in this case the light, transmitted to port 2, contains a relatively wide spectrum of frequencies as compared to the first structure. Figure 6 shows the maximum of the relative transmission of the structure at port 1 (star symbols) and at port 2 (dot symbols) as a function of the lattice distortion. From Fig. 6 we note that at port 2, the transmission coefficient shows nonmonotonic behavior with a wide maximum at $\Delta r/a\sim 0.15$ (dot symbols), while at port 1 the transmission is almost unchanged for $0<\Delta r/a<0.2$. Figure 7 presents the pattern of the z component of the electric field in the frequency domain for the resonant frequency $\omega=0.354$ at $\Delta r/a=0$ (a), 0.13 (b), and for the resonant frequencies $\omega=0.351$ (c), and 0.361 (d) at $\Delta r/a=0.13$. The figure demonstrates that for the undistorted lattice, the light propagates along the straight line [Fig. 7(a)], while for the distorted lattice, the guided modes with different frequencies propagate along different waveguide arms.

We will analyze this structure in a similar way as the previous one. The first question that arises when we compare the frequency spectrum inside the bad gap for these two structures (Figs. 2 and 5) is the following: what makes these two structures so different? The answer follows from the geometry. We note that for the second structure [inset of Fig. 5(a)], the corner defect does not belong to any arm. Because of this, the frequency spectrum of the corner defect, in the first approximation, can be considered to be independent of the spectrum of all the three arms even for small lattice distortions. As a result, the transmission at port 2 has a wide maximum both as function of the frequency and lattice distortion. For the B_2 distortion with $\Delta r>0$, the $|p_x+p_y\rangle$ state

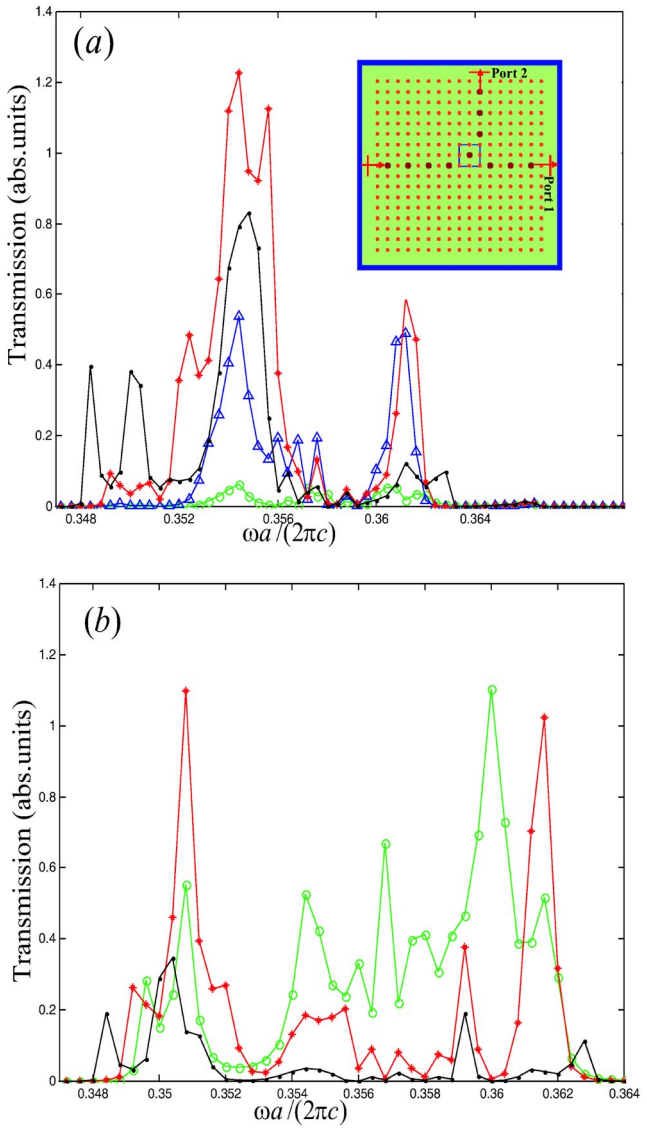

FIG. 5. (Color online) The relative transmission intensity inside the band gap for the structures shown in the inset with $\Delta r/a=0$ (circle marker), 0.05 (triangular marker), 0.13 (star marker), and 0.25 (dotted marker) at port 2(a) and for the structure with $\Delta r/a=0$ (circle marker), 0.13 (star marker), 0.25 (dotted marker) at port 1 (b). The inset shows the structure studied with the B_2 distortion of the corner cell. The Jahn-Teller corner cell, the perfect matched boundaries, as well as the source and two ports are overlaid.

goes down in frequency and $|p_x-p_y\rangle$ state goes up. Since each of the arms contains a finite number of sites n, the band spectrum of each of them should be described by n number of resonant levels. Then the maximum of the transmission will be reached if the $|p_x+p_y\rangle$ state of the corner cell overlaps in frequency with the two resonant levels in arm 1 and arm 3. For a concrete geometry with four defect sites in arm 1 and three sites in arm 3, the resonant levels in both arms overlap at the edges of the band $\omega_{\|}^{m}=\omega_0\pm\beta_{\|}$. By analogy with the first structure, we draw the conclusion that the transmission at port 2 will be maximum at $\Delta r\sim 2\beta_{\|}/v^{B2}$. Now, using the known value $v^{B2}\sim 0.05$, obtained from the supercell plane-wave calculation in Ref. 8, we get $\Delta r\sim 0.2$, in

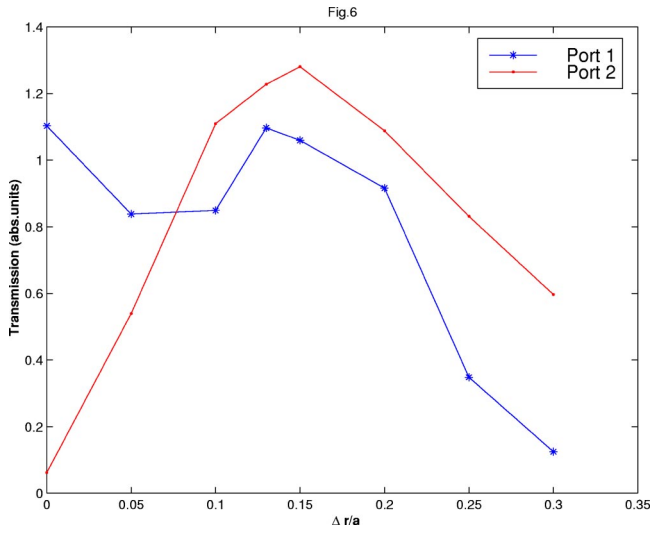

FIG. 6. Computed maximum of the relative transmission coefficient of the structure in the inset of Fig. 5(a) as a function of the lattice distortion at port 1 (star markers) and at port 2 (dot markers).

reasonable agreement with the FDTD simulations. On the other hand, another smaller peak in the transmission spectrum is observed at port 2 at the high-frequency edge of the spectrum for the lattice distortion $\Delta r/a=0.13$ [the line with star markers in Fig. 5(a)]. It corresponds to the frequency matching between another resonant level $\omega_{\|}^{m}=\omega_0+\beta_{\|}$ and the corner defect $|p_x-p_y\rangle$ state. Patterns of the E_z field for the resonant frequency $\omega=0.354$ at $\Delta r/a=0$. and 0.13 presented in Figs. 7(a) and (b) provides support for this analysis.

As for the transmission at port 1, its amplitude does not change significantly with distortion (Fig. 6). But the peak of the transmission is shifted [Fig. 5(b)]. This correlates with the shift of the $|p_x\pm p_y\rangle$ states of the corner defect. The

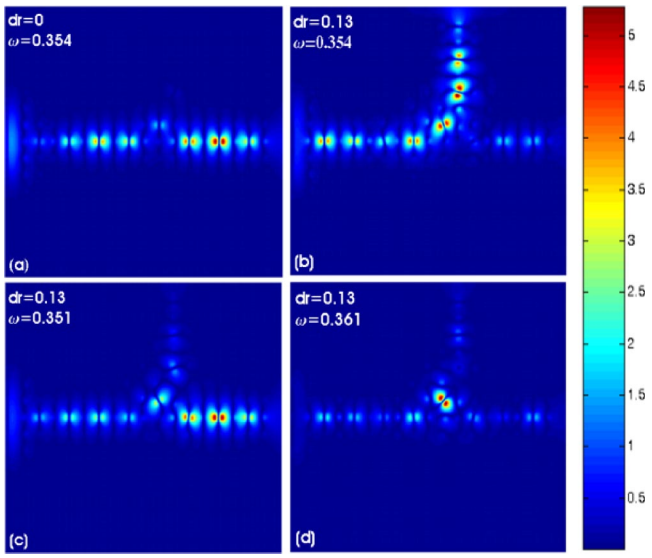

FIG. 7. (Color online) The pattern of the z component of the electric field in the frequency domain for the resonant frequency $\omega=0.354$ at $\Delta r/a=0$ (a), 0.13 (b), and for the resonant frequencies $\omega=0.351$ (c) and 0.361 (d) at $\Delta r/a=0.13$.

maximum of the transmission in frequency is controlled by the splitting of the corner degenerate defect state. The split $|p_x \pm p_y\rangle$ states scan the resonant levels of the p_x band of arms 1 and 2. As soon as the split $|p_x \pm p_y\rangle$ state overlaps with the two resonant levels in both arms, the transmission will be maximum. The width of the transmission peak is determined by the width of the split corner defect states. This explains the two sharp extremes of the transmission at port 1 at $\Delta r/a = 0.13$ [the line with star markers in Fig. 5(b)]. They exactly correspond to an overlap in the frequency of the $|p_x \pm p_y\rangle$ split corner states with the high- and low-frequency edges of the p_x band of arms 1 and 2. The data for the pattern of the E_z field presented in Figs. 7(c) and (d) support this statement.

IV. CONCLUSION

In conclusion, in this paper we have studied the effect of splitting the doubly degenerate defect level of a square two-dimensional photonic lattice by the Jahn-Teller distortion of the lattice. The effect shows a linear scaling of the magnitude of frequency splitting with the amplitude of the lattice distortion. The symmetry of the split photon defect mode is shown to be driven by the symmetry of the lattice distortion. We show that the effect can be used for tunable light propagation through 90°-bend waveguides. A coupled cavity T-junction waveguide structures with either B_1 or B_2 perturbation of the corner defect at the junction has been considered as an example. We show that it is possible to tune the propagation of the light along the couple cavity waveguide if we place a Jahn-Teller cell at the corner and then gradually change then the magnitude of the lattice distortion of this cell. Both structures have been shown to work as tunable waveguide devices. In the case of the undistorted corner cell, light propagates mostly along the straight arm of both the structures studied. For the distorted corner cell, the frequency spectrum of the structures is different. We show that for the structure with B_1 mode distortion, light transport can be directed either along the straight arm or into the bent arm, with the frequency dependence of the transmitted light showing a very sharp peak $\sim 10^{-3}$ (in relative units). For the waveguide devices operating at the light wavelength of 1.55 μm, this corresponds to the width of the transmission peak of ~ 2 nm. From these data, we can conclude that the structure with working B_1 mode can work as a switching waveguide with high-frequency selectivity. In the case of the structure with B_2 distortion, we demonstrate that the guided modes with different frequencies propagate along different waveguide arms. The frequency spectrum of the transmitted light in the structure with working B_2 mode is much wider than for the structure with working B_1 mode. We explain this effect within the framework of the tight-binding theory. We emphasize that the frequency region of the transmission peak can be easily controlled by the lattice distortion and by the geometry of the structures.

A straightforward way to implement this device concept is to provide a local control of the lattice distortion by piezoelectric elements built directly beneath or above the waveguide corner. The rod displacements involved for devices at 1.55-μm wavelength light are of order of 200 nm, which are achievable using present day piezoelectrics.[17]

ACKNOWLEDGMENTS

We would like to acknowledge the support from the Center for Collective Phenomena in Restricted Geometries (Penn State MRSEC) under NSF Grant No. DMR-00800190, National Science Foundation Grant No. ECS-9988685. We thank the Materials Simulation Center (Penn State) for the provision of the computer facilities.

[1] *Photonic Crystals and Light Localization in the 21st Century*, edited by C. M. Soukoulis, NATO Science Series No. 563 (Kluwer Academic Publishers, Dordrecht, 2001).
[2] A. Mekis, J.C. Chen, I. Kurland, S. Fan, P.R. Villeneuve, and J.D. Joannopoulos, Phys. Rev. Lett. **77**, 3787 (1996).
[3] A. Yariv, Y. Xu, R.K. Lee, and A. Scherer, Opt. Lett. **24**, 711 (1999).
[4] E. Ozbay, M. Bayindir, I. Bulu, and E. Cubukcu, IEEE J. Quantum Electron. **38**, 837 (2002).
[5] M. Bayindir, B. Temelkuran, and E. Ozbay, Phys. Rev. B **61**, R11 855 (2000); M. Bayindir, S. Tanriseven, and E. Ozbay, Appl. Phys. A: Mater. Sci. Process. **72**, 117 (2001).
[6] H. Takeda and K. Yoshino, Phys. Rev. B **67**, 073106 (2003).
[7] L. D. Landau and E. M. Liphshitz, *Quantum Mechanics* (Nauka, Moscow, 1974).
[8] N. Malkova, S. Kim, and V. Gopalan, Phys. Rev. B **68**, 045105 (2003).
[9] N. Malkova, S. Kim, and V. Gopalan, Appl. Phys. Lett. **83**, 1509 (2003).
[10] N. Malkova, S. Kim, and V. Gopalan, J. Phys.: Condens. Matter **15**, 4535 (2003).
[11] K. Sakoda and H. Shiroma, Phys. Rev. B **56**, 4830 (1997).
[12] I. B. Bersuker, *The Jahn-Teller Effect and Vibronic Interactions in Modern Chemistry* (Plenum, New York, 1983).
[13] A. Taflove and S. C. Hagness, *Computational Electrodynamics: The Finite-Difference Time-Domain Method* (Artech House, Boston, 2000).
[14] A. Talneau, L. Le Gouezigou, N. Bouadma, M. Kafesaki, and C.M. Soukoulis, Appl. Phys. Lett. **80**, 547 (2002).
[15] We note that the transmission coefficient for some of the frequencies exceeds 1. This is an artifact well known for the numerical FDTD simulations of the complex nonperiodical system. It has been discussed in a number of papers; see, for example, A. Mekis, J.C. Chen, I. Kurland, S. Fan, P.R. Villeneuve, and J.D. Joannopoulos, Phys. Rev. Lett. **77**, 3787 (1996).
[16] U. Peschel, A.L. Reynolds, B. Arredondo, F. Lederer, P.J. Roberts, T.F. Krauss, and P.J.I. de Maagt, IEEE J. Quantum Electron. **38**, 830 (2002).
[17] S. Kim and V. Gopalan, Appl. Phys. Lett. **78**, 3015 (2001).